Article

A Concept of Assessment of LIV Tests with *THESEUS* Using the Gamma-Ray Bursts Detected by *Fermi*/GBM

Anastasia Tsvetkova [1,2,*], Luciano Burderi [1,3,4], Alessandro Riggio [1,3,5] and Andrea Sanna [1,3,4] and Tiziana Di Salvo [6]

1   Dipartimento di Fisica, Universitá degli Studi di Cagliari, SP Monserrato-Sestu, km 0.7, 09042 Monserrato, Italy; burderi@dsf.unica.it (L.B.); alessandro.riggio@dsf.unica.it (A.R.); andrea.sanna@dsf.unica.it (A.S.)
2   Ioffe Institute, Politekhnicheskaya 26, 194021 St. Petersburg, Russia
3   INFN, Sezione di Cagliari, Cittadella Universitaria, 09042 Monserrato, Italy
4   INAF—Osservatorio Astronomico di Cagliari, Via della Scienza 5, 09047 Selargius, Italy
5   INAF—Istituto di Astrofisica Spaziale e Fisica Cosmica di Palermo, Via U. La Malfa 153, 90146 Palermo, Italy
6   Dipartimento di Fisica e Chimica, Universitá degli Studi di Palermo, Via Archirafi 36, 90123 Palermo, Italy; tiziana.disalvo@unipa.it
*   Correspondence: tsvetkova.lea@gmail.com or tsvetkova@mail.ioffe.ru

Abstract: According to Einstein's special relativity theory, the speed of light in a vacuum is constant for all observers. However, quantum gravity effects could introduce its dispersion depending on the energy of photons. The investigation of the spectral lags between the gamma-ray burst (GRB) light curves recorded in distinct energy ranges could shed light on this phenomenon: the lags could reflect the variation of the speed of light if it is linearlydependent on the photon energy and a function of the GRB redshift. We propose a methodology to start investigating the dispersion law of light propagation in a vacuum using GRB light curves. This technique is intended to be fully exploited using the GRB data collected with *THESEUS*.

Keywords: gamma-ray bursts; GRBs as cosmological probes and test-bench for fundamental physics; GRBs: past, present and future experiments and missions

1. Introduction

According to Einstein's special relativity theory, a proper length is Lorentz-contracted by a factor of $\gamma^{-1} = [1 - (v/c)^2]^{1/2}$ as observed from the reference frame moving at speed v relative to the rest frame. However, various spacetime theories, e.g., some string or loop quantum gravity theories (see, e.g., [1–3]), imply the existence of a minimum spatial length of the order of the Plank length $l_{Pl} = \sqrt{G\hbar/c^3} = 1.6 \times 10^{-33}$ cm [4]. Lorentz invariance is a fundamental property of both the standard model of particle physics and general relativity. In general relativity, a locally inertial reference frame where the Lorentz symmetry is fulfilled can always be chosen. Some quantum gravity (QG) theories predict the Lorentz invariance violation (LIV) at the Planck energy scale ($E_{Pl} = \sqrt{\hbar c^5/G} \simeq 1.22 \times 10^{19}$ GeV) as there exists a minimum spatial length $l_{min} = \alpha l_{Pl}$ (where $\alpha \sim 1$ is a dimensionless constant inherent to a particular spacetime theory), which, e.g., in the string theories, corresponds to the string length. Therefore, the Lorentz contraction is limited by this spatial scale (see [4] for a review).

There are several frameworks implying LIV, e.g., string theory [5,6], noncommutative spacetime [7,8], Brane worlds [9], Hořava–Lifshitz gravity [10]. LIV was considered in the gravitational context for the first time in [11], where the so-called standard model extension was developed. The Bumblebee[1] models, which are the simplest cases of theories including the spontaneous breaking of Lorentz symmetry, are effective field QG theories describing a vector field with a non-zero vacuum expectation value and involving the

vacuum condensate [5,6]. The spontaneous symmetry breaking preserves both the geometric constraints and conservation laws or quantities required by the general relativity theory or Riemannian geometry. Regarding gravity, LIV can happen if a vector field ruled by a potential exhibiting a minimum rolls to its vacuum expectation value, similar to the Higgs mechanism [11]. This "bumblebee" vector thus takes an explicit (four-dimensional) orientation, and preferred-frame effects may emerge [12]. The generalized uncertainty principle (GUP) states that, in quantum theory, if the quantities are incompatible, they are mutually dependent, and measuring one observable may yield some information about its incompatible partners. GUP is based on a momentum-dependent modification of the standard dispersion relation, which is supposed to produce LIV [13,14]. See, e.g., [15–21] for recent advances in the Bumblebee and GUP models.

One of the LIV effects, relevant to astrophysics, is the existence of a dispersion law for the photon speed **c** (see, e.g., [22]). However, LIV is not a mandatory property of all QG theories: in some of them, e.g., in the spacetime uncertainty principle [23] or in the quantum spacetime [24], LIV is not expected. Despite photon velocity dispersion, the Lorentz invariance is not violated and the dispersion law is a second-order effect relative to the ratio of the photon energy to the QG energy scale. To obtain an idea of the nature of the speed of light dispersion due to LIV, e.g., within the Liouville string approach, one can consider a vacuum as a non-trivial medium containing "foamy" quantum gravity fluctuations whose origin can be imagined as processes that involve the pair creation of virtual black holes. In this concept, one can verify that the massless particles of different energies can excite vacuum fluctuations differently as they propagate through the quantum gravity medium, producing a non-trivial dispersion relation of Lorentz "non-covariant" form, similarly to the thermal medium [25]. For more details regarding this concept, see, e.g., [26].

Since gamma-ray bursts (GRBs) are characterized by high-energy emission, large cosmological distances, and temporal variability at short ($\lesssim$10 ms) timescales, they have been applied as powerful tools in LIV searches (see, e.g., [25,27–49]) for more than two decades. In [25], it was first suggested to test LIV using a comparison of the arrival times of GRB photons detected in distinct energy ranges. In [29,30,50], the authors exploited the spectral lag between high-energy ($\sim$31 GeV) and low-energy photons of GRB 090510 to derive lower limits on the linear and quadratic QG energy: $E_{QG,1} > (1-10) \times E_{Pl} = 1.22 \times (10^{19} - 10^{20})$ GeV and $E_{QG,2} > (1-10) \times E_{Pl} = 1.3 \times 10^{11}$ GeV, respectively. In [51], $E_{QG} > 10^{18}$ GeV was obtained based on the observation of GRB 080916C. For GRB 190114C [52], the linear and quadratic LIV were constrained using the time delays of TeV photons: $E_{QG,1} > 0.58 \times 10^{19}$ GeV ($E_{QG,1} > 0.55 \times 10^{19}$ GeV) and $E_{QG,2} > 0.63 \times 10^{11}$ GeV ($E_{QG,1} > 0.56 \times 10^{11}$ GeV) for the subluminal (superluminal) case [43]. In [53], the authors constrained the linear and quadratic LIV for the set of 32 *Fermi*/GBM GRBs with known redshifts and characterized by the positive-to-negative transition of the spectral lag: $E_{QG,1} = 1.5 \times 10^{14}$ GeV for the linear case and $E_{QG,2} = 8 \times 10^5$ GeV for the quadratic case.

The phenomenon of GRBs remains puzzling, although much progress has been made. Both the light curves and the spectra among GRBs vary significantly. It is generally believed that collisions between relativistic shells ejected from an active central engine produce pulses in GRB light curves [54]. The collision of the slower-moving shell with the second, faster shell ejected later produces a shock that dissipates internal energy and accelerates the particles that emit the GRB radiation. As of now, two "physical" classes of GRBs are distinguished (see, e.g., [55]): the merger-origin Type I GRBs [56–59], which are usually short, with a duration of less than 2 s [60,61], and spectrally hard, and the collapser-origin Type II GRBs [62–65], characterized by longer durations.

The spectral lag, which is known as the difference in arrival time between high-energy and low-energy photons, is a common phenomenon occurring during the GRB prompt emission phase [66–69] and in high-energy astrophysics in general (e.g., [67,70]). The authors of [71] were the first to analyze the spectral lags of GRBs. It was found that a soft lag, i.e., the hard photons arriving first, dominates in long GRBs [67,69,72,73], and

some GRBs have significantly different spectral lags in early and late epochs [74]. It was shown that the lags are correlated with the GRB luminosity [67] and the jet break times in afterglow light curves [75]; the spectral lags of long GRBs are correlated with the pulse duration, while the spectral lags of short GRBs are not [76]. The GRB spectral lags can be explained within several physical models, such as the curvature effect of a relativistic jet and rapidly expanding spherical shell [77–81]. Regardless of its physical origin, a spectral lag is an important GRB parameter as it may help to distinguish between long and short GRBs: long bursts have large lags, while short bursts have relatively smaller or negligible lags [82–84].

To show the feasibility of the search for the dispersion of the speed of the light in the data collected by THESEUS [85], one can start performing similar research using the data of already commissioned missions. In this paper, we describe a methodology for the testing of the dispersion of the light speed, and we intend to apply it to the *Fermi*/GBM data and the set of GRBs with known redshifts. The paper is organized as follows. We start with a brief description of the instrumentation and data in Section 2. The methodology that involves constraining LIV using GRBs is described in Section 3. In Section 4, we discuss the *THESEUS* mission in the context of the LIV tests using GRBs. Section 5 concludes the paper.

2. Instrumentation and Data

Among several space-based detectors able to collect GRB data, the most prolific are *Swift*/BAT (BAT; [86]), *Fermi*/GBM (GBM; [87]), and Konus-*Wind* (KW; [88]). More details regarding the BAT, GBM, KW, and other GRB detectors' design and performance can be found in [89]. However, since *Swift*/BAT collects GRB data in a narrow energy band of 15–350 keV, and Konus-*Wind* records GRB light curves in three fixed energy windows, the *Fermi/GBM* GRB time histories seem to be the most suitable for the testing of the speed of light variance.

Launched in June 2008, the *Fermi* Gamma-Ray Space Telescope [90] harbors two scientific instruments: the Gamma-Ray Burst Monitor (GBM) and the Large Area Telescope (LAT; [91]). The LAT covers the 30 MeV–300 GeV band, while the GBM, intended to detect and study GRBs, is sensitive within the 8 keV–30 MeV energy range, extending the spectral band over which bursts are observed downwards to the hard X-ray range. GBM comprises twelve NaI(Tl) detectors covering an energy range of 8 keV^{-1} MeV and two bismuth-germanate (BGO) scintillation detectors sensitive within the 150 keV to 30 MeV band that observe the whole sky not occluded by the Earth (>8 sr).

The primary scientific data produced by GBMs can be summarized as a time history and spectra, which are provided as temporally pre-binned (CTIME and CSPEC) or temporally unbinned time tagged events (TTE). These data types are produced as "snippets" for every trigger and are also provided continuously. The CTIME data are collected in 8 energy channels with a 256 ms time resolution, while the CSPEC data are recorded in 128 channels with an 8.192 s time resolution. TTEs for each detector are recorded with time precision down to 2 μs, in 128 energy channels, matching the CSPEC ones, which gives an excellent opportunity to bin the data in time and energy in a suitable way. From 2008 through November 2012, TTE were available only during a 330 s interval: from 30 s before the burst trigger to 300 s after the burst trigger. Since November 2012, GBM flight software has produced a new data type, continuous TTE (CTTE), available at all times that the instrument is operating.

To date, the GBM has triggered almost 3500 GRBs, among which almost 3000 have $T_{90} > 2$ s.

3. Methodology

We start the research by computing the redshifts and the rest-frame spectral lags for all GBM-triggered GRBs. Then, thanks to the central limit theorem, we can consider the distribution of the lags as normal and compute the mean and variance. The large number

of "measurements" is expected to significantly increase the accuracy of the spectral lags and constraints on E_{QG}. Another approach would be to constrain the QG energy (see Section 3.1) first and then estimate its mean values and variance.

3.1. Brief Introduction to the Basics of the Speed of Light Variance

The velocity dispersion law for photons can be expressed as a function of its observer-frame energy E_{obs} in units of the QG energy scale E_{QG}, at which the quantum nature of gravity becomes important:

$$v_{phot}/c - 1 = \xi \left(\frac{E_{obs}}{E_{QG}} \right)^n,$$ (1)

where v_{phot} is the group velocity of a photon wave-packet, $E_{QG} = \zeta m_{Pl} c^2 = \zeta E_{Pl}$, $m_{Pl} = 2.176 \times 10^{-5}$ g is the Planck mass, $\zeta \sim \alpha^{-1} \sim 1$ expresses the significance of the QG effects, $\xi \sim \pm 1$ is a dimensionless constant inherent to a particular QG theory, and the index n denotes the order of the first relevant term of the small parameter $\left(\frac{E_{obs}}{E_{QG}} \right)$. This expression takes into account that high-energy photons can travel faster (superluminal, $\xi = +1$) or slower (subluminal, $\xi = -1$) than low-energy ones [92].

The difference in the arrival times of photons emitted at the same time in the same place is

$$\Delta t_{QG} = \xi \left(\frac{D_{trav}}{c} \right) \left(\frac{\Delta E_{obs}}{E_{QG}} \right)^n,$$ (2)

where D_{trav} is the comoving distance traversed by a massless particle, emitted at redshift z and traveling down to redshift 0.

3.2. Observed Spectral Lag as a Function of Redshift

For a given observer-frame energy E_{obs}, the total spectral lag $\tau_{total,obs}(E_{obs}, z)$ can be split into two terms:

$$\tau_{total,obs}(E_{obs}, z) = \tau_{int,obs}(E_{obs}, z) + \tau_{QG,obs}(E_{obs}, z),$$ (3)

where $\tau_{int,obs}$ is the observed intrinsic spectral lag, which corresponds to the intrinsic rest-frame lag

$$\tau_{int,rf}(E_{obs}) = \tau_{int,obs}(E_{rf})/(1+z)$$ (4)

induced by the GRB central engine emission mechanism and assumed to be independent of the photon source redshift z. $\tau_{QG,obs}$ is the lag induced by the QG effects discussed above, and and E_{rf} is the photon energy in the rest frame of its source. Following [93], $\tau_{QG,obs}$ can be expressed as a function of the GRB rest-frame energy:

$$\tau_{QG}(E_{rf}, z) = \xi \left(\frac{1}{H_0} \right) \left(\frac{E_{rf}}{\zeta E_{pl}} \right)^n \left(\frac{1+n}{2} \right) \left(\frac{1}{1+z} \right)^n \times$$
$$\times \int_0^z \frac{(1+z')^n dz'}{\sqrt{\Omega_m (1+z')^3 + \Omega_\Lambda}},$$ (5)

where H_0 is the Hubble constant, Ω_m is the matter density parameter, and Ω_Λ is the dark energy density parameter, i.e., the parameters of the standard ΛCDM model.

Experimentally, the total observed spectral lag $\tau_{total,obs}(E_{rf}, z)$ can be computed by cross-correlating the GRB light curves recorded in the redshift-dependent energy windows corresponding to the fixed rest-frame energy windows as $E_{obs} = E_{rf}/(1+z)$, with the GRB light curve collected at the lowest possible energy channel, where the lag induced by QG is negligible, e.g., it is $\sim\mu$s in the 5–20 keV energy range, while, in the higher-energy bands, it is $\sim$ms.

The total observed spectral lag $\tau_{\text{total, obs}}(E_{\text{rf}}, z)$ should follow the relation obtained by inserting Equations (4) and (5) into Equation (3):

$$\tau_{\text{total, obs}}(E_{\text{rf}}, z) = \tau_{\text{int, obs}}(E_{\text{rf}}) +$$

$$\xi\left(\frac{1}{H_0}\right)\left(\frac{E_{\text{rf}}}{\zeta E_{\text{pl}}}\right)^n \left(\frac{1+n}{2}\right)\left(\frac{1}{1+z}\right)^n \int_0^z \frac{(1+z')^n dz'}{\sqrt{\Omega_m(1+z')^3 + \Omega_\Lambda}}. \quad (6)$$

The transformation of spectral lags from the observer frame back to the rest frame[2] can be performed by dividing by the redshift factor $(1+z)$:

$$\tau_{\text{total, rf}}(E_{\text{rf}}, z) = \tau_{\text{total, obs}}(E_{\text{rf}}, z)/(1+z). \quad (7)$$

Thus, the GRB rest-frame spectral lag obeys the following relation:

$$\tau_{\text{total, rf}}(E_{\text{rf}}, z) = \frac{\tau_{\text{int, obs}}(E_{\text{rf}})}{(1+z)} +$$

$$\xi\left(\frac{1}{H_0}\right)\left(\frac{E_{\text{rf}}}{\zeta E_{\text{pl}}}\right)^n \left(\frac{1+n}{2}\right)\left(\frac{1}{1+z}\right)^{n+1} \int_0^z \frac{(1+z')^n dz'}{\sqrt{\Omega_m(1+z')^3 + \Omega_\Lambda}}. \quad (8)$$

Let us define a function

$$u(z) = \left(\frac{1+n}{2}\right)\left(\frac{1}{1+z}\right)^{n+1} \int_0^z \frac{(1+z')^n dz'}{\sqrt{\Omega_m(1+z')^3 + \Omega_\Lambda}}. \quad (9)$$

Then, the experimentally determined lag $\tau_{\text{total, obs}}(E_{\text{rf}}, z)$ will follow the relation

$$\tau_{\text{total,rf}}(E_{\text{rf}}, z) = \tau_{\text{int,rf}}(E_{\text{rf}}) + \xi\left(\frac{1}{H_0}\right)\left(\frac{E_{\text{rf}}}{\zeta E_{\text{pl}}}\right)^n u(z). \quad (10)$$

The dependence of $\tau_{\text{total, rf}}(E_{\text{rf}}, z)$ on $u(z)$ is expected to be linear, with the intercept corresponding to the intrinsic lag and the slope proportional to the ratio of the rest-frame photon energy to the QG energy ζE_{pl} raised to the n-th power, which is the first significant term in the series expansion of the quantum gravity dispersion relation. An argument in support of the independence of $\tau_{\text{int, rf}}$ from z is the absence of the prominent cosmological evolution of GRB energetics [89,94], which indicates that the GRB central engine does not evolve significantly with z. However, if $\tau_{\text{int, rf}}$ is dependent on z, one can fit both $\tau_{\text{int, rf}}(z)$ and $\tau_{\text{QG}}(z)$ simultaneously to the data, as was done in [53].

In [53], it was found that the behavior of the lags follows some key statistical properties described in terms of log-normal and Gaussian distributions around average values. These empirical functions describing the spectral lags (as a function of energy) for each of the 32 *Fermi*/GBM GRBs in the sample of bursts with known redshifts that exhibit the lag transition phenomenon are shown in Figure 1 (as derived from Figure 1 of [53]). In the method proposed here, we make the reasonable assumption that the intrinsic lags (that dominate in magnitude over the small delays induced by QG effects; see the upper limits for the first- and second-order QG delays shown as blue and orange curves in Figure 1) do not correlate with the redshift as the distance of a given GRB from us does not affect the emission properties in, e.g., the fireball model. This means that, averaging over a large sample of GRBs at different redshifts, the intrinsic delays will cluster around the common value that defines the intrinsic average rest-frame lag.
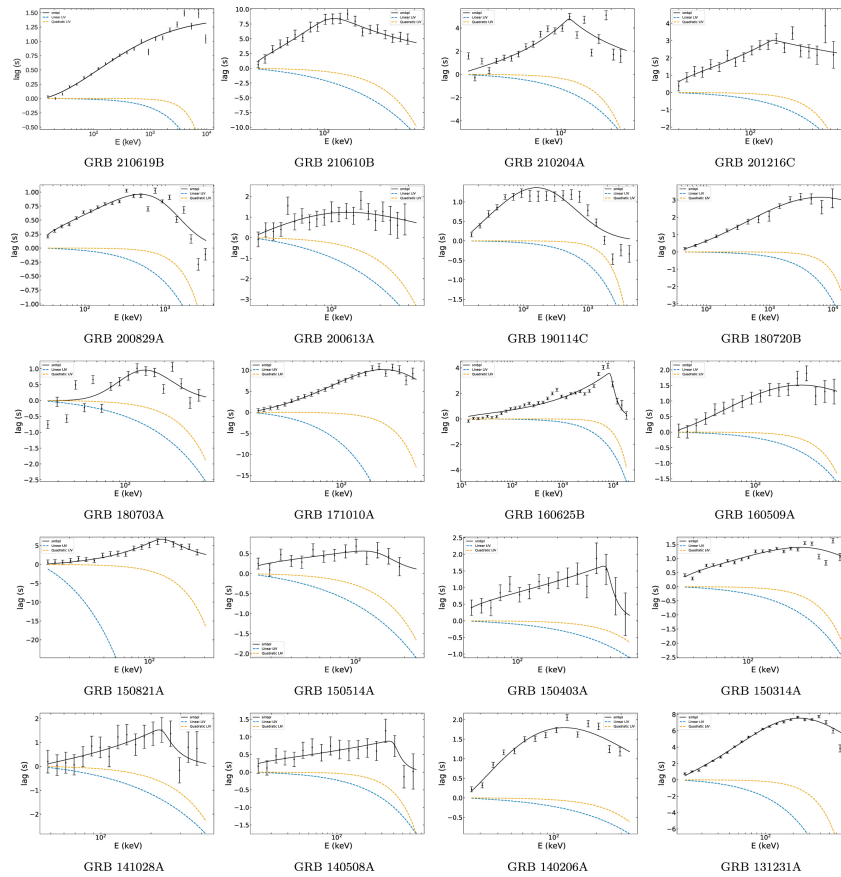
Figure 1. The dependence of the spectral lag on the energy window for the GRB sample studied in [53]. The fits with a smoothly broken power law (SBPL) are shown by black solid lines. Blue and orange dotted lines denote the maximally allowed LIV-induced lags in linear and quadratic cases, thereby defining the lower limits on the QG energy. This figure is adapted from Figure 1 from [53] (see Section 3 of this work for details). ©AAS. Reproduced with permission.

3.3. The Technique of Averaging over the Sample

Relation (10) shows that, for a given GRB rest-frame energy $E_{\rm rf}$, the lag $\tau_{\rm total,\,rf}(E_{\rm rf})$ depends only on the GRB redshift z through the function $u(z)$ defined in Equation (9). Therefore, fixing $E_{\rm rf}$ for an ensemble of N GRBs with known redshift, one can compute the function $\tau_{\rm total,\,rf}(E_{\rm rf})$ from the observed data for all GRBs of the ensemble, i.e., it is possible to obtain a set of N experimentally computed values of $\tau_{\rm total,\,rf}(E_{\rm rf})$. This ensemble of N values can be fitted as a function of $u(z)$ through Equation (10) to obtain the best fit values of the intrinsic lag in the GRB rest frame $\tau_{\rm int,\,rf}$, and the coefficient of the QG-induced delay at the GRB rest-frame energy $E_{\rm rf}$

$$
\begin{cases}
\left[\tau_{int,rf}(E_{\rm rf})\right]_{\rm BEST} \\
\text{and} \\
\left[\xi\left(\dfrac{1}{H_0}\right)\left(\dfrac{E_{\rm rf}}{\zeta E_{\rm pl}}\right)^n\right]_{\rm BEST} = \\
\left[\xi\left(\dfrac{1}{H_0}\right)\left(\alpha\dfrac{E_{\rm rf}}{E_{\rm pl}}\right)^n\right]_{\rm BEST} = \left[\phi(\alpha E_{\rm rf})\right]_{\rm BEST}
\end{cases}
. \qquad (11)
$$

Once the values of $[\phi(\alpha E_{\rm rf})]_{\rm BEST}$ are obtained for all $E_{\rm rf}$, these values can be plotted as a function of $s(E_{\rm rf}) = (E_{\rm rf}/E_{\rm pl})^n$ and subsequently linearly fitted through the equation

$$\phi(\alpha E_{\mathrm{rf}}) = \left(\frac{\alpha^n}{H_0}\right) s(E_{\mathrm{rf}}) = \Delta_{\mathrm{QG}}\, s(E_{\mathrm{rf}}), \tag{12}$$

to obtain the best fit value of the strength of the QG effect $\Delta_{\mathrm{QG}} = \alpha^n / H_0$. We note that this technique allows us to combine the whole ensemble of N GRBs to obtain a unique measure of the strength of the QG effect, whose uncertainty $\sigma_{\Delta_{\mathrm{QG}}}$, in the absence of other systematic errors, only depends on the (Poissonian) statistics of the whole ensemble of N GRBs and therefore improves as the inverse square root of N:

$$\sigma_{\Delta_{\mathrm{QG}}} \propto \frac{1}{\sqrt{N}}. \tag{13}$$

Consequently, the precision of the measurement of the QG effect's strength can be improved by increasing the size of the analyzed sample.

3.4. GRB Intrinsic Spectral Lags vs. Quantum Gravity Effects

The GRB spectral lag can be caused by a mixture of two effects: the QG one and the one inherent to the fireball model. The latter is due to the curvature effect, i.e., the kinematic effect caused by the fact that the observer looks at an increasingly off-axis annulus area relative to the line-of-sight [77–79,95–100]. Softer low-energy radiation comes from the off-axis annulus area with smaller Doppler factors and is delayed for the observer with respect to on-axis emission due to the geometric curvature of the shell.

A competing hypothesis is that the traditional view based on the high-latitude emission "curvature effect" of a relativistic jet cannot explain spectral lags. Instead, spectral peaks should be swept across the observing energy range in a specific manner to account for the observed spectral lags. A simple physical model that implies synchrotron radiation from a rapidly expanding outflow can explain GRB spectral lags [81]. This model requires the following conditions to be fulfilled: (1) the emission radius has to be large (over several 10^{14} cm from the central engine), in the optically thin region, well above the photosphere; (2) the γ-ray photon spectrum is curved (as observed); (3) the magnetic field strength in the emitting region decreases with the radius as the region expands in space, which is consistent with an expanding jet; and (4) the emission region itself undergoes rapid bulk acceleration as the prompt emission is produced. These requirements are consistent with a Poynting-flux-dominated jet abruptly dissipating magnetic energy at a large distance from the engine. The aforementioned theories successfully explain the positive spectral lags. Nevertheless, the rarely observed negative lags remain a more intriguing phenomenon that can be used to infer the different radiation mechanisms [101,102] or emission regions [103] of low- and high-energy photons.

For a given GRB, the intrinsic delay inherent to the GRB emission could mimic the genuine quantum gravity effect, making these two effects difficult to disentangle. However, currently, there is no evidence for a correlation between the GRB intrinsic delays and the distances to its sources. For example, in [94,104], where the largest sample of GRBs with known redshifts detected by a single instrument in a wide energy range is studied, the significance of the cosmological evolution of GRB energetics is $\lesssim 2\sigma$. Meanwhile, the delays induced by a photon dispersion law are proportional both to the light travel distance (a function of redshift) and to the differences in the energy of the photons. This dual dependence on energy and redshift could be the unique feature of a genuine QG effect. As suggested in [105], given an adequate collection area, GRBs, once their redshifts are known, are potentially excellent tools to search for the first-order dispersion law for photons.

3.5. Computation of Spectral Lags

To avoid distortions due to the fact that the shape of the light curve changes with the energy, we suggest fixing the energy channels in which the light curves are recorded to certain values in the rest frame. In this case, the corresponding observer-frame values of the channel boundaries will be $E_{\mathrm{obs}} = E_{\mathrm{rest}} / (1 + z)$, i.e., redshift-dependent. The first step to

test the LIV effects with the suggested technique would be apply it to the GBM data. Thus, we propose to use the following energy bands to record the light curves. Given the 9 keV lower boundary of the GBM spectral window, one has to select the rest-frame channels starting from, at least, 60 keV, to allow for bursts with redshifts up to $z = 5$. This boundary can be shifted towards a higher value to allow high-redshift GRBs to contribute to the study. However, we should mention that the majority of GRBs have redshifts $z < 5$ (see Figure 2). Some examples of the pseudo-logarithmic channels that could be used are 60–100 keV, 100–160 keV, 160–250 keV, 250–400 keV, 400–600 keV, 600–900 keV, or 60–80 keV, 80–100 keV, 100–130 keV, 130–160 keV, 160–200 keV, 200–250 keV, 250–320 keV, 320–400 keV, 400–500 keV, 500–650 keV, 650–900 keV. We found these numbers of channels to be reasonable in terms of SNR based on the research of [53], carried out for 32 *Fermi*/GBM GRBs.

Since the GRB energetics are usually considered on the logarithmic scale, we suggest adopting the geometric mean of the lower and upper boundaries of an energy band, $E_{phot} = \sqrt{E_{min} \times E_{max}}$, as a proxy for the average energy of photons in the given range.
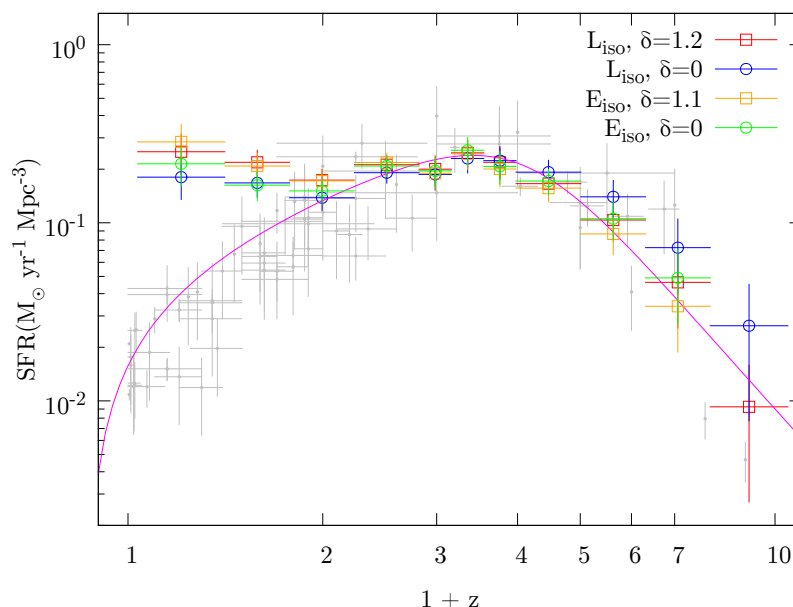

Figure 2. The cosmological GRB formation rate (GRBFR) derived in [104], superposed onto the star formation rate (SFR) data from the literature. The gray points show the SFR data from [106–109]. The marked line denotes the SFR approximation from [110]. The GRBFR normalization is equal for all four data sets and the GRBFR points have been shifted arbitrarily to match the SFR at $(1-z) \sim 3.5$. Figure 5b from [104]. ©AAS. Reproduced with permission.

Since the spectral lag distributions of the short and long GRBs significantly differ [76], and these two types of bursts belong to distinct classes of progenitors, they have different intrinsic spectral lags. Thus, we suggest studying them separately.

3.6. Obtaining GRB Redshifts

Since the suggested technique of testing LIV using GRBs strongly relies on prior knowledge of the burst redshift, it is necessary either to measure it directly from the observations in optics or estimate it using the prompt emission parameters. GRB redshift measurements based on the detection of emission lines or absorption features of GRB host galaxies imposed on the afterglow continuum, or performed photometrically, are widespread. However, there are other methods to obtain the redshift estimates, e.g., the "pseudo-redshift" (pseudo-z) technique based on the spectral properties of GRB prompt high-energy emission [111], using well-known correlations such as, for example, the Norris correlation (spectral lag vs. isotropic peak luminosity; [67]), the Amati correlation (rest-frame peak energy vs. isotropic energy release; [112]), the isotropic peak luminosity vs.

temporal variability correlation [113,114], the Yonetoku (the rest-frame peak energy vs. the isotropic peak luminosity; [115]) correlation, etc., or the method of searching for a minimum on the intrinsic hydrogen column density versus the redshift plane (see, e.g., [116]).

Nowadays, the machine learning (ML) approach to redshift estimation is becoming popular in astrophysics (see, e.g., [117–120]). Supervised ML is a data mining method based on prior knowledge of a "training" data set, on which we can build models predicting the parameter under consideration, a "validation" set, which provides an unbiased evaluation of a model's fit while tuning the model's hyperparameters, and a "test" data set necessary for an unbiased evaluation of the final model fit.

Considering only spectroscopic and photometric redshifts, there were $\gtrsim$420 GRBs with reliably measured redshifts by the middle of 2022 (for a list of GRBs with measured redshifts, see [94,104,121–123], the Gamma-Ray Burst Online Index[3], Jochen Greiner's GRB table [4], and the references therein). Using one of the aforementioned techniques, one can estimate the redshift of any burst based on its temporal or spectral parameters and energetics. For example, [115,124,125] used various correlations to obtain unknown GRB redshifts from GRB observables, while [126] used the random forest algorithm to estimate GRB redshifts.

4. Discussion

THESEUS is a mission aimed at increasing the discovery rate of the high-energy transient phenomena over the entirety of cosmic history and fully exploiting GRBs to explore the early Universe [85,127]. *THESEUS* is likely to become a cornerstone of multi-messenger and time-domain astrophysics thanks to its exceptional payload, providing wide and deep sky monitoring in a broad energy range (0.3 keV–20 MeV); focusing capabilities in the soft X-ray band, providing large grasp and a high angular resolution; and onboard near-IR capabilities for immediate transient identification and redshift determination.

The *THESEUS* payload is planned to include the following instrumentation: (1) the X-Gamma-Ray Imaging Spectrometer (XGIS, 2 keV–20 MeV): a set of two coded-mask cameras using monolithic X-gamma-ray detectors based on bars of silicon diodes coupled with a crystal scintillator, granting a $\sim$2 sr field of view (FoV) and source location accuracy of $\sim$10$'$ in the 2–150 keV band, as well as a >4 sr FoV at energies > 150 keV, with a few μs timing resolution; (2) a Soft X-Ray Imager (SXI, 0.3–5 keV): a set of two lobster-eye telescope units, covering a total FOV of $\sim$0.5 sr with source location accuracy $\lesssim$ 2$'$; (3) an infrared telescope (IRT, 0.7–1.8 μm): a 0.7 m class IR telescope with a 15$'$ × 15$'$ FOV, for a fast response, with both imaging (I, Z, Y, J, and H) and spectroscopic (resolving power, R$\sim$400, through 2$'$ × 2$'$ grism) capabilities.

Thanks to the unique combination of a wide 0.3 keV–10 MeV energy range, remarkable sensitivity, and exceptionally high counting statistics, *THESEUS* heralds a new era in the multi-wavelength studies of GRBs, providing the community with a sample of GRBs with known redshifts of unprecedented size, which, in turn, will not only allow the use of GRBs as cosmological tools but also shed light on one of the most challenging aspects of QG theory, the systematic study of which is still beyond the current instrumental capabilities. The capability of *THESEUS* to detect and localize GRBs, as well as measure their redshifts, will essentially surpass those of the current missions.

The left panel of Figure 3 shows the expected detection rate of long GRBs by *THESEUS* compared with observed GRBs. The orange histogram depicts the cumulative distribution of the GRBs detected by the SXI and/or XGIS (the bursts with measured *z* are marked in purple), while the blue histogram presents the distribution of GRBs with known redshifts detected from 2005 to the end of 2020. The distribution of the GRBs detected by *THESEUS* was acquired based on the anticipated IRT capabilities and on the assumption of a ground follow-up rate of 50% for the GRBs at *z* < 5. It is noticeable that *THESEUS* is expected to detect an order of magnitude more bursts than *Swift* does, especially in the high-redshift domain (*z* > 6) [128]. It is expected that the redshifts for the majority of GRBs detected by *THESEUS* will be measured (onboard or on the ground). The cumulative distribution

plotted in the right panel of Figure 3 represents the annual detection rate of short GRBs by XGIS, not corrected for mission observation efficiency. *THESEUS* is supposed to acquire a statistically significant sample of short GRBs, including high-redshift ($z \lesssim 4$–5) events. Considering that the distribution of the spectral lags of short GRBs and long GRBs differs significantly, advances in research on short GRBs are very important for such sophisticated studies of the QG effects as we discuss in this paper. Thus, the sample of GRBs with measured redshifts obtained by THESEUS is the most promising for the application of the described technique to study LIV.
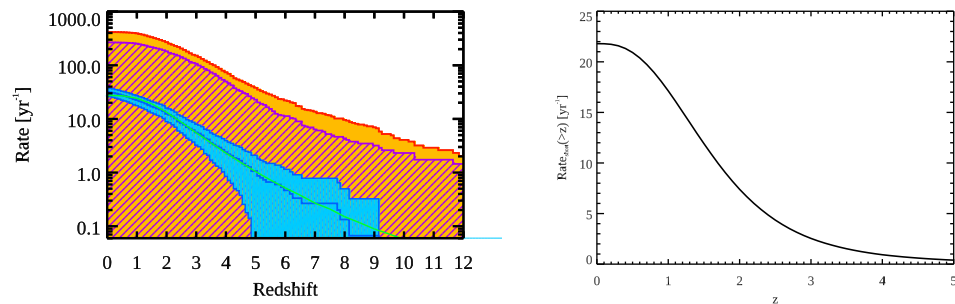

Figure 3. Left plot: Observed GRBs with known redshifts measured in 2005–2020 (blue line and filled cyan area representing 1σ uncertainty) superimposed on the anticipated frequency of detection of long GRBs by *THESEUS* (orange histogram). The purple hatched histogram shows the GRBs that are expected to have a redshift measured by either *THESEUS* or ground-based facilities' telescopes. The model that fits the observed distribution used to make predictions for *THESEUS* is represented by the green curve. *THESEUS* is expected to detect one to two orders of magnitude more GRBs than Swift at any redshift, and most importantly in the high-redshift range ($z > 6$). Right plot: Cumulative redshift distribution of short GRBs detectable with *THESEUS*/XGIS per year of mission. Theoretically, short GRBs can be detected at high redshifts $z > 4$ with a rate of ~ 1 event per year. This figure is adopted from [128].

5. Conclusions

Various QG theories predict LIV, which can manifest itself as the dispersion of the speed of light. The method that we propose to disentangle and constrain the QG delays from the intrinsic spectral lags in GRB light curves is based on the assumption of the constancy of the rest-frame intrinsic spectral lags and on the linear dependence of the GRB spectral lag on both the photon energy and function of the GRB redshift. The ability to collect a large sample of GRBs with known redshifts is crucial for this type of study, as the precision of the QG effect measurement can be improved by expanding the data set. Currently, redshifts are measured spectroscopically or photometrically for $\lesssim 500$ GRBs. Thus, indirect estimates of the redshifts from the prompt emission observables are necessary to obtain a large GRB sample for LIV studies using the commissioned instruments. The sample of GRBs collected by *Fermi*/GBM could provide a promising opportunity to apply the aforementioned technique, thanks to its extensive trigger statistics ($\gtrsim 3500$ GRBs up to date) and sophisticated data acquired with a high temporal and spectral resolution, which could allow precise measurements of the rest-frame spectral lags.

The *THESEUS* mission is likely to initiate a breakthrough in this field of fundamental physics as, thanks to the combination of its unique characteristics, the observatory will collect one order of magnitude more samples of GRBs with known redshifts than are currently available, which will not only allow the use of GRBs as cosmological tools but will also enable us to constrain the QG theories. Moreover, thanks to its capability to detect the GRB emission in the relatively soft energy band of 0.3–5 keV, *THESEUS* could provide a unique opportunity not only to constrain the empirical and physical GRB models but also to expand the data range, providing more accurate constraints on the QG energy from the lag-energy plane. Due to its high sensitivity, *THESEUS* will also allow advances in the study of short GRBs; in particular, XGIS will be able to detect short GRBs up to z~4–5,

which is important as the spectral lags of short GRBs essentially differ from the ones of long bursts. Thus, the *THESEUS* mission could make a significant contribution to the study of the QG effects using GRBs.

Data Availability Statement: Not applicable.

Conflicts of Interest: The authors declare no conflict of interest.

Abbreviations

The following abbreviations are used in this manuscript:

GRB	Gamma-ray burst
GUP	Generalized uncertainty principle
FoV	Field of view
LIV	Lorentz invariance violation
QG	Quantum gravity

Notes

[1] The name of the model was inspired by the insect, whose ability to fly has been questioned theoretically.

[2] This value reflects only the mathematical transformation from the observer frame to the rest frame as, at the moment of emission of two photons, the QG lag between them equals zero.

[3] https://sites.astro.caltech.edu/grbox/grbox.php, accessed on 2 May 2023.

[4] https://www.mpe.mpg.de/~jcg/grbgen.html, accessed on 2 May 2023.

References

1. Rovelli, C.; Smolin, L. Knot theory and quantum gravity. *Phys. Rev. Lett.* **1988**, *61*, 1155–1158. [CrossRef] [PubMed]
2. Rovelli, C.; Smolin, L. Loop space representation of quantum general relativity. *Nuclear Phys. B* **1990**, *331*, 80–152. [CrossRef]
3. Rovelli, C. Loop Quantum Gravity. *Living Rev. Relativ.* **1998**, *1*, 1.
4. Hossenfelder, S. Minimal Length Scale Scenarios for Quantum Gravity. *Living Rev. Relativ.* **2013**, *16*, 2.
5. Kostelecký, V.A.; Samuel, S. Spontaneous breaking of Lorentz symmetry in string theory. *Phys. Rev. D* **1989**, *39*, 683–685. [CrossRef]
6. Kostelecký, V.A.; Samuel, S. Gravitational phenomenology in higher-dimensional theories and strings. *Phys. Rev. D* **1989**, *40*, 1886–1903. [CrossRef]
7. Carroll, S.M.; Harvey, J.A.; Kostelecký, V.A.; Lane, C.D.; Okamoto, T. Noncommutative Field Theory and Lorentz Violation. *Phys. Rev. Lett.* **2001**, *87*, 141601.
8. Ferrari, A.F.; Gomes, M.; Nascimento, J.R.; Passos, E.; Petrov, A.Y.; da Silva, A.J. Lorentz violation in the linearized gravity. *Phys. Lett. B* **2007**, *652*, 174–180.
9. Santos, V.; Almeida, C.A.S. On gravity localization under Lorentz violation in warped scenario. *Phys. Lett. B* **2013**, *718*, 1114–1118.
10. Hořava, P. Quantum gravity at a Lifshitz point. *Phys. Rev. D* **2009**, *79*, 084008.
11. Kostelecký, V.A. Gravity, Lorentz violation, and the standard model. *Phys. Rev. D* **2004**, *69*, 105009.
12. Bertolami, O.; Páramos, J. Vacuum solutions of a gravity model with vector-induced spontaneous Lorentz symmetry breaking. *Phys. Rev. D* **2005**, *72*, 044001.
13. Tawfik, A.N.; Magdy, H.; Ali, A.F. Lorentz invariance violation and generalized uncertainty principle. *Phys. Part. Nucl. Lett.* **2016**, *13*, 59–68.

14. Lambiase, G.; Scardigli, F. Lorentz violation and generalized uncertainty principle. *Phys. Rev. D* **2018**, *97*, 075003.
15. Kanzi, S.; Sakallı, İ. GUP modified Hawking radiation in bumblebee gravity. *Nuclear Phys. B* **2019**, *946*, 114703.
16. Övgün, A.; Jusufi, K.; Sakallı, I. Exact traversable wormhole solution in bumblebee gravity. *Phys. Rev. D* **2019**, *99*, 024042.
17. Kanzi, S.; Sakallı, I. Greybody radiation and quasinormal modes of Kerr-like black hole in Bumblebee gravity model. *Eur. Phys. J. C* **2021**, *81*, 501.
18. Delhom, A.; Nascimento, J.R.; Olmo, G.J.; Petrov, A.Y.; Porfírio, P.J. Metric-affine bumblebee gravity: Classical aspects. *Eur. Phys. J. C* **2021**, *81*, 287.
19. Gogoi, D.J.; Dev Goswami, U. Quasinormal modes and Hawking radiation sparsity of GUP corrected black holes in bumblebee gravity with topological defects. *J. Cosmol. Astropart. Phys.* **2022**, *2022*, 029.
20. Gogoi, D.J.; Dev Goswami, U. Tideless traversable wormholes surrounded by cloud of strings in f(R) gravity. *J. Cosmol. Astropart. Phys.* **2023**, *2023*, 027. [CrossRef]
21. Neves, J.C.S. Kasner cosmology in bumblebee gravity. *Ann. Phys.* **2023**, *454*, 169338.
22. Amelino-Camelia, G. Are We at the Dawn of Quantum-Gravity Phenomenology? In *Toward Quantum Gravity*; Kowalski-Glikman, J., Ed.; Springer: Berlin/Heidelberg, Germany, 2000; Volume 541, p. 1.
23. Burderi, L.; Di Salvo, T.; Iaria, R. Quantum clock: A critical discussion on spacetime. *Phys. Rev. D* **2016**, *93*, 064017.
24. Sanchez, N.G. New Quantum Structure of Space-Time. *Gravit. Cosmol.* **2019**, *25*, 91–102.
25. Amelino-Camelia, G.; Ellis, J.; Mavromatos, N.E.; Nanopoulos, D.V.; Sarkar, S. Tests of quantum gravity from observations of γ-ray bursts. *Nature* **1998**, *393*, 763–765. Erratum in *Nature* **1998**, *395*, 525.
26. Amelino-Camelia, G.; Ellis, J.; Mavromatos, N.E.; Nanopoulos, D.V. Distance Measurement and Wave Dispersion in a Liouville-String Approach to Quantum Gravity. *Int. J. Mod. Phys. A* **1997**, *12*, 607–623.
27. Ellis, J.; Mavromatos, N.E.; Nanopoulos, D.V.; Sakharov, A.S. Quantum-gravity analysis of gamma-ray bursts using wavelets. *Astron. Astrophys.* **2003**, *402*, 409–424. [CrossRef]
28. Ellis, J.; Mavromatos, N.E.; Nanopoulos, D.V.; Sakharov, A.S.; Sarkisyan, E.K.G. Robust limits on Lorentz violation from gamma-ray bursts. *Astropart. Phys.* **2006**, *25*, 402–411.
29. Abdo, A.A.; Ackermann, M.; Ajello, M.; Asano, K.; Atwood, W.B.; Axelsson, M.; Baldini, L.; Ballet, J.; Barbiellini, G.; Baring, M.G.; et al. A limit on the variation of the speed of light arising from quantum gravity effects. *Nature* **2009**, *462*, 331–334.
30. Vasileiou, V.; Granot, J.; Piran, T.; Amelino-Camelia, G. A Planck-scale limit on spacetime fuzziness and stochastic Lorentz invariance violation. *Nat. Phys.* **2015**, *11*, 344–346. [CrossRef]
31. Zhang, S.; Ma, B.Q. Lorentz violation from gamma-ray bursts. *Astropart. Phys.* **2015**, *61*, 108–112.
32. Pan, Y.; Gong, Y.; Cao, S.; Gao, H.; Zhu, Z.H. Constraints on the Lorentz Invariance Violation with Gamma-Ray Bursts via a Markov Chain Monte Carlo Approach. *Astrophys. J.* **2015**, *808*, 78.
33. Xu, H.; Ma, B.Q. Light speed variation from gamma ray burst GRB 160509A. *Phys. Lett. B* **2016**, *760*, 602–604.
34. Xu, H.; Ma, B.Q. Light speed variation from gamma-ray bursts. *Astropart. Phys.* **2016**, *82*, 72–76.
35. Chang, Z.; Li, X.; Lin, H.N.; Sang, Y.; Wang, P.; Wang, S. Constraining Lorentz invariance violation from the continuous spectra of short gamma-ray bursts. *Chin. Phys. C* **2016**, *40*, 045102.
36. Wei, J.J.; Zhang, B.B.; Shao, L.; Wu, X.F.; Mészáros, P. A New Test of Lorentz Invariance Violation: The Spectral Lag Transition of GRB 160625B. *Astrophys. J. Lett.* **2017**, *834*, L13.
37. Ganguly, S.; Desai, S. Statistical significance of spectral lag transition in GRB 160625B. *Astropart. Phys.* **2017**, *94*, 17–21.
38. Liu, Y.; Ma, B.Q. Light speed variation from gamma ray bursts: Criteria for low energy photons. *Eur. Phys. J. C* **2018**, *78*, 825.
39. Zou, X.B.; Deng, H.K.; Yin, Z.Y.; Wei, H. Model-independent constraints on Lorentz invariance violation via the cosmographic approach. *Phys. Lett. B* **2018**, *776*, 284–294.
40. Ellis, J.; Konoplich, R.; Mavromatos, N.E.; Nguyen, L.; Sakharov, A.S.; Sarkisyan-Grinbaum, E.K. Robust constraint on Lorentz violation using Fermi-LAT gamma-ray burst data. *Phys. Rev. D* **2019**, *99*, 083009.
41. Wei, J.J. New constraints on Lorentz invariance violation with polarized gamma-ray bursts. *Mon. Not. RAS* **2019**, *485*, 2401–2406.
42. Pan, Y.; Qi, J.; Cao, S.; Liu, T.; Liu, Y.; Geng, S.; Lian, Y.; Zhu, Z.H. Model-independent Constraints on Lorentz Invariance Violation: Implication from Updated Gamma-Ray Burst Observations. *Astrophys. J.* **2020**, *890*, 169.
43. Acciari, V.A.; Ansoldi, S.; Antonelli, L.A.; Arbet Engels, A.; Baack, D.; Babić, A.; Banerjee, B.; Barres de Almeida, U.; Barrio, J.A.; Becerra González, J.; et al. Bounds on Lorentz Invariance Violation from MAGIC Observation of GRB 190114C. *Phys. Rev. Lett.* **2020**, *125*, 021301.
44. Du, S.S.; Lan, L.; Wei, J.J.; Zhou, Z.M.; Gao, H.; Jiang, L.Y.; Zhang, B.B.; Liu, Z.K.; Wu, X.F.; Liang, E.W.; et al. Lorentz Invariance Violation Limits from the Spectral-lag Transition of GRB 190114C. *Astrophys. J.* **2021**, *906*, 8.
45. Agrawal, R.; Singirikonda, H.; Desai, S. Search for Lorentz Invariance Violation from stacked Gamma-Ray Burst spectral lag data. *J. Cosmol. Astropart. Phys.* **2021**, *2021*, 029.
46. Wei, J.J.; Wu, X.F. Testing fundamental physics with astrophysical transients. *Front. Phys.* **2021**, *16*, 44300.
47. Bartlett, D.J.; Desmond, H.; Ferreira, P.G.; Jasche, J. Constraints on quantum gravity and the photon mass from gamma ray bursts. *Phys. Rev. D* **2021**, *104*, 103516.
48. Xiao, S.; Xiong, S.L.; Wang, Y.; Zhang, S.N.; Gao, H.; Zhang, Z.; Cai, C.; Yi, Q.B.; Zhao, Y.; Tuo, Y.L.; et al. A Robust Estimation of Lorentz Invariance Violation and Intrinsic Spectral Lag of Short Gamma-Ray Bursts. *Astrophys. J. Lett.* **2022**, *924*, L29. [CrossRef]

49. Desai, S.; Agrawal, R.; Singirikonda, H. Search for Lorentz invariance violation using Bayesian model comparison applied to Xiao et al. GRB spectral lag catalog. *Eur. Phys. J. C* **2023**, *83*, 63.

50. Vasileiou, V.; Jacholkowska, A.; Piron, F.; Bolmont, J.; Couturier, C.; Granot, J.; Stecker, F.W.; Cohen-Tanugi, J.; Longo, F. Constraints on Lorentz invariance violation from Fermi-Large Area Telescope observations of gamma-ray bursts. *Phys. Rev. D* **2013**, *87*, 122001.

51. Abdo, A.A.; Ackermann, M.; Arimoto, M.; Asano, K.; Atwood, W.B.; Axelsson, M.; Baldini, L.; Ballet, J.; Band, D.L.; Barbiellini, G.; et al. Fermi Observations of High-Energy Gamma-Ray Emission from GRB 080916C. *Science* **2009**, *323*, 1688. [CrossRef] [PubMed]

52. MAGIC Collaboration.; Acciari, V.A.; Ansoldi, S.; Antonelli, L.A.; Arbet Engels, A.; Baack, D.; Babić, A.; Banerjee, B.; Barres de Almeida, U.; Barrio, J.A.; et al. Teraelectronvolt emission from the γ-ray burst GRB 190114C. *Nature* **2019**, *575*, 455–458.

53. Liu, Z.K.; Zhang, B.B.; Meng, Y.Z. Spectral Lag Transition of 32 Fermi Gamma-Ray Bursts and Their Application on Constraining Lorentz Invariance Violation. *Astrophys. J.* **2022**, *935*, 79.

54. Rees, M.J.; Meszaros, P. Unsteady Outflow Models for Cosmological Gamma-Ray Bursts. *Astrophys. J. Lett.* **1994**, *430*, L93.

55. Zhang, B.; Zhang, B.B.; Virgili, F.J.; Liang, E.W.; Kann, D.A.; Wu, X.F.; Proga, D.; Lv, H.J.; Toma, K.; Mészáros, P.; et al. Discerning the Physical Origins of Cosmological Gamma-ray Bursts Based on Multiple Observational Criteria: The Cases of z = 6.7 GRB 080913, z = 8.2 GRB 090423, and Some Short/Hard GRBs. *Astrophys. J.* **2009**, *703*, 1696–1724.

56. Blinnikov, S.I.; Novikov, I.D.; Perevodchikova, T.V.; Polnarev, A.G. Exploding Neutron Stars in Close Binaries. *Sov. Astron. Lett.* **1984**, *10*, 177–179.

57. Paczynski, B. Gamma-ray bursters at cosmological distances. *Astrophys. J. Lett.* **1986**, *308*, L43–L46. [CrossRef]

58. Eichler, D.; Livio, M.; Piran, T.; Schramm, D.N. Nucleosynthesis, neutrino bursts and γ-rays from coalescing neutron stars. *Nature* **1989**, *340*, 126–128. [CrossRef]

59. Paczynski, B. Cosmological gamma-ray bursts. *Acta Astron.* **1991**, *41*, 257–267.

60. Mazets, E.P.; Golenetskii, S.V.; Ilinskii, V.N.; Panov, V.N.; Aptekar, R.L.; Gurian, I.A.; Proskura, M.P.; Sokolov, I.A.; Sokolova, Z.I.; Kharitonova, T.V. Catalog of cosmic gamma-ray bursts from the KONUS experiment data. *Astrophys. Space Sci.* **1981**, *80*, 3–83. [CrossRef]

61. Kouveliotou, C.; Meegan, C.A.; Fishman, G.J.; Bhat, N.P.; Briggs, M.S.; Koshut, T.M.; Paciesas, W.S.; Pendleton, G.N. Identification of Two Classes of Gamma-Ray Bursts. *Astrophys. J. Lett.* **1993**, *413*, L101. [CrossRef]

62. Woosley, S.E. Gamma-Ray Bursts from Stellar Mass Accretion Disks around Black Holes. *Astrophys. J.* **1993**, *405*, 273. [CrossRef]

63. Paczyński, B. Are Gamma-Ray Bursts in Star-Forming Regions? *Astrophys. J. Lett.* **1998**, *494*, L45–L48.

64. MacFadyen, A.I.; Woosley, S.E. Collapsars: Gamma-Ray Bursts and Explosions in "Failed Supernovae". *Astrophys. J.* **1999**, *524*, 262–289.

65. Woosley, S.E.; Bloom, J.S. The Supernova Gamma-Ray Burst Connection. *Annu. Rev. Astron Astrophys.* **2006**, *44*, 507–556.

66. Norris, J.P.; Share, G.H.; Messina, D.C.; Dennis, B.R.; Desai, U.D.; Cline, T.L.; Matz, S.M.; Chupp, E.L. Spectral Evolution of Pulse Structures in Gamma-Ray Bursts. *Astrophys. J.* **1986**, *301*, 213. [CrossRef]

67. Norris, J.P.; Marani, G.F.; Bonnell, J.T. Connection between Energy-dependent Lags and Peak Luminosity in Gamma-Ray Bursts. *Astrophys. J.* **2000**, *534*, 248–257.

68. Band, D.L. Gamma-Ray Burst Spectral Evolution through Cross-Correlations of Discriminator Light Curves. *Astrophys. J.* **1997**, *486*, 928–937.

69. Chen, L.; Lou, Y.Q.; Wu, M.; Qu, J.L.; Jia, S.M.; Yang, X.J. Distribution of Spectral Lags in Gamma-Ray Bursts. *Astrophys. J.* **2005**, *619*, 983–993.

70. Zhang, Y.H.; Treves, A.; Celotti, A.; Chiappetti, L.; Fossati, G.; Ghisellini, G.; Maraschi, L.; Pian, E.; Tagliaferri, G.; Tavecchio, F. Four Years of Monitoring Blazar PKS 2155-304 with BeppoSAX: Probing the Dynamics of the Jet. *Astrophys. J.* **2002**, *572*, 762–785.

71. Cheng, L.X.; Ma, Y.Q.; Cheng, K.S.; Lu, T.; Zhou, Y.Y. The time delay of gamma-ray bursts in the soft energy band. *Astron. Astrophys.* **1995**, *300*, 746.

72. Wu, B.; Fenimore, E. Spectral Lags of Gamma-Ray Bursts From Ginga and BATSE. *Astrophys. J. Lett.* **2000**, *535*, L29–L32.

73. Norris, J.P.; Bonnell, J.T.; Kazanas, D.; Scargle, J.D.; Hakkila, J.; Giblin, T.W. Long-Lag, Wide-Pulse Gamma-Ray Bursts. *Astrophys. J.* **2005**, *627*, 324–345.

74. Hakkila, J.; Giblin, T.W. Quiescent Burst Evidence for Two Distinct Gamma-Ray Burst Emission Components. *Astrophys. J.* **2004**, *610*, 361–367. [CrossRef]

75. Salmonson, J.D.; Galama, T.J. Discovery of a Tight Correlation between Pulse Lag/Luminosity and Jet-Break Times: A Connection between Gamma-Ray Bursts and Afterglow Properties. *Astrophys. J.* **2002**, *569*, 682–688.

76. Yi, T.; Liang, E.; Qin, Y.; Lu, R. On the spectral lags of the short gamma-ray bursts. *Mon. Not. RAS* **2006**, *367*, 1751–1756.

77. Ioka, K.; Nakamura, T. Peak Luminosity-Spectral Lag Relation Caused by the Viewing Angle of the Collimated Gamma-Ray Bursts. *Astrophys. J. Lett.* **2001**, *554*, L163–L167.

78. Shen, R.F.; Song, L.M.; Li, Z. Spectral lags and the energy dependence of pulse width in gamma-ray bursts: Contributions from the relativistic curvature effect. *Mon. Not. RAS* **2005**, *362*, 59–65.

79. Lu, R.J.; Qin, Y.P.; Zhang, Z.B.; Yi, T.F. Spectral lags caused by the curvature effect of fireballs. *Mon. Not. RAS* **2006**, *367*, 275–289.

80. Shenoy, A.; Sonbas, E.; Dermer, C.; Maximon, L.C.; Dhuga, K.S.; Bhat, P.N.; Hakkila, J.; Parke, W.C.; Maclachlan, G.A.; Eskandarian, A.; et al. Probing Curvature Effects in the Fermi GRB 110920. *Astrophys. J.* **2013**, *778*, 3.

81. Uhm, Z.L.; Zhang, B. Toward an Understanding of GRB Prompt Emission Mechanism. I. The Origin of Spectral Lags. *Astrophys. J.* **2016**, *825*, 97.

82. Norris, J.P. Gamma-Ray Bursts: The Time Domain. *Astrophys. Space Sci.* **1995**, *231*, 95–102. [CrossRef]

83. Ryde, F. Interpretations of gamma-ray burst spectroscopy. I. Analytical and numerical study of spectral lags. *Astron. Astrophys.* **2005**, *429*, 869–879. [CrossRef]

84. Norris, J.P.; Bonnell, J.T. Short Gamma-Ray Bursts with Extended Emission. *Astrophys. J.* **2006**, *643*, 266–275.

85. Amati, L.; O'Brien, P.; Götz, D.; Bozzo, E.; Tenzer, C.; Frontera, F.; Ghirlanda, G.; Labanti, C.; Osborne, J.P.; Stratta, G.; et al. The THESEUS space mission concept: Science case, design and expected performances. *Adv. Space Res.* **2018**, *62*, 191–244.

86. Gehrels, N.; Chincarini, G.; Giommi, P.; Mason, K.O.; Nousek, J.A.; Wells, A.A.; White, N.E.; Barthelmy, S.D.; Burrows, D.N.; Cominsky, L.R.; et al. The Swift Gamma-Ray Burst Mission. *Astrophys. J.* **2004**, *611*, 1005–1020. [CrossRef]

87. Meegan, C.; Lichti, G.; Bhat, P.N.; Bissaldi, E.; Briggs, M.S.; Connaughton, V.; Diehl, R.; Fishman, G.; Greiner, J.; Hoover, A.S.; et al. The Fermi Gamma-ray Burst Monitor. *Astrophys. J.* **2009**, *702*, 791–804.

88. Aptekar, R.L.; Frederiks, D.D.; Golenetskii, S.V.; Ilynskii, V.N.; Mazets, E.P.; Panov, V.N.; Sokolova, Z.J.; Terekhov, M.M.; Sheshin, L.O.; Cline, T.L.; et al. Konus-W Gamma-Ray Burst Experiment for the GGS Wind Spacecraft. *Space Sci. Rev.* **1995**, *71*, 265–272. [CrossRef]

89. Tsvetkova, A.; Svinkin, D.; Karpov, S.; Frederiks, D. Key Space and Ground Facilities in GRB Science. *Universe* **2022**, *8*, 373. [CrossRef]

90. Thompson, D.J.; Wilson-Hodge, C.A. Fermi Gamma-ray Space Telescope. *arXiv* **2022**, arXiv:2210.12875.

91. Atwood, W.B.; Abdo, A.A.; Ackermann, M.; Althouse, W.; Anderson, B.; Axelsson, M.; Baldini, L.; Ballet, J.; Band, D.L.; Barbiellini, G.; et al. The Large Area Telescope on the Fermi Gamma-Ray Space Telescope Mission. *Astrophys. J.* **2009**, *697*, 1071–1102.

92. Amelino-Camelia, G.; Smolin, L. Prospects for constraining quantum gravity dispersion with near term observations. *Phys. Rev. D* **2009**, *80*, 084017.

93. Jacob, U.; Piran, T. Lorentz-violation-induced arrival delays of cosmological particles. *J. Cosmol. Astropart. Phys.* **2008**, *2008*, 031.

94. Tsvetkova, A.; Frederiks, D.; Golenetskii, S.; Lysenko, A.; Oleynik, P.; Pal'shin, V.; Svinkin, D.; Ulanov, M.; Cline, T.; Hurley, K.; et al. The Konus-Wind Catalog of Gamma-Ray Bursts with Known Redshifts. I. Bursts Detected in the Triggered Mode. *Astrophys. J.* **2017**, *850*, 161.

95. Fenimore, E.E.; Madras, C.D.; Nayakshin, S. Expanding Relativistic Shells and Gamma-Ray Burst Temporal Structure. *Astrophys. J.* **1996**, *473*, 998.

96. Salmonson, J.D. On the Kinematic Origin of the Luminosity-Pulse Lag Relationship in Gamma-Ray Bursts. *Astrophys. J. Lett.* **2000**, *544*, L115–L117.

97. Kumar, P.; Panaitescu, A. Afterglow Emission from Naked Gamma-Ray Bursts. *Astrophys. J. Lett.* **2000**, *541*, L51–L54.

98. Qin, Y.P. Doppler effect of gamma-ray bursts in the fireball framework. *Astron. Astrophys.* **2002**, *396*, 705–713. [CrossRef]

99. Qin, Y.P.; Zhang, Z.B.; Zhang, F.W.; Cui, X.H. Characteristics of Profiles of Gamma-Ray Burst Pulses Associated with the Doppler Effect of Fireballs. *Astrophys. J.* **2004**, *617*, 439–460.

100. Dermer, C.D. Curvature Effects in Gamma-Ray Burst Colliding Shells. *Astrophys. J.* **2004**, *614*, 284–292.

101. Li, Z. Prompt GeV Emission from Residual Collisions in Gamma-Ray Burst Outflows: Evidence from Fermi Observations of Grb 080916c. *Astrophys. J.* **2010**, *709*, 525–534.

102. Zhang, B.B.; Zhang, B.; Liang, E.W.; Fan, Y.Z.; Wu, X.F.; Pe'er, A.; Maxham, A.; Gao, H.; Dong, Y.M. A Comprehensive Analysis of Fermi Gamma-ray Burst Data. I. Spectral Components and the Possible Physical Origins of LAT/GBM GRBs. *Astrophys. J.* **2011**, *730*, 141.

103. Toma, K.; Wu, X.F.; Mészáros, P. An Up-Scattered Cocoon Emission Model of Gamma-Ray Burst High-Energy Lags. *Astrophys. J.* **2009**, *707*, 1404–1416.

104. Tsvetkova, A.; Frederiks, D.; Svinkin, D.; Aptekar, R.; Cline, T.L.; Golenetskii, S.; Hurley, K.; Lysenko, A.; Ridnaia, A.; Ulanov, M. The Konus-Wind Catalog of Gamma-Ray Bursts with Known Redshifts. II. Waiting-Mode Bursts Simultaneously Detected by Swift/BAT. *Astrophys. J.* **2021**, *908*, 83.

105. Burderi, L.; Di Salvo, T.; Riggio, A.; Gambino, A.F.; Sanna, A.; Fiore, F.; Amarilli, F.; Amati, L.; Ambrosino, F.; Amelino-Camelia, G.; et al. GrailQuest and HERMES: Hunting for gravitational wave electromagnetic counterparts and probing space-time quantum foam. In Proceedings of the Society of Photo-Optical Instrumentation Engineers (SPIE) Conference Series, 2020, Volume 11444, p. 114444.

106. Hopkins, A.M. On the Evolution of Star-forming Galaxies. *Astrophys. J.* **2004**, *615*, 209–221.

107. Bouwens, R.J.; Illingworth, G.D.; Labbe, I.; Oesch, P.A.; Trenti, M.; Carollo, C.M.; van Dokkum, P.G.; Franx, M.; Stiavelli, M.; González, V.; et al. A candidate redshift z ≈ 10 galaxy and rapid changes in that population at an age of 500 Myr. *Nature* **2011**, *469*, 504–507.

108. Hanish, D.J.; Meurer, G.R.; Ferguson, H.C.; Zwaan, M.A.; Heckman, T.M.; Staveley-Smith, L.; Bland-Hawthorn, J.; Kilborn, V.A.; Koribalski, B.S.; Putman, M.E.; et al. The Survey for Ionization in Neutral Gas Galaxies. II. The Star Formation Rate Density of the Local Universe. *Astrophys. J.* **2006**, *649*, 150–162.

109. Thompson, R.I.; Eisenstein, D.; Fan, X.; Dickinson, M.; Illingworth, G.; Kennicutt, R.C.J. Star Formation History of the Hubble Ultra Deep Field: Comparison with the Hubble Deep Field-North. *Astrophys. J.* **2006**, *647*, 787–798.

110. Li, L.X. Star formation history up to z = 7.4: Implications for gamma-ray bursts and cosmic metallicity evolution. *Mon. Not. RAS* **2008**, *388*, 1487–1500.
111. Atteia, J.L. A simple empirical redshift indicator for gamma-ray bursts. *Astron. Astrophys.* **2003**, *407*, L1–L4. [CrossRef]
112. Amati, L.; Frontera, F.; Tavani, M.; in't Zand, J.J.M.; Antonelli, A.; Costa, E.; Feroci, M.; Guidorzi, C.; Heise, J.; Masetti, N.; et al. Intrinsic spectra and energetics of BeppoSAX Gamma-Ray Bursts with known redshifts. *Astron. Astrophys.* **2002**, *390*, 81–89. [CrossRef]
113. Reichart, D.E.; Lamb, D.Q.; Fenimore, E.E.; Ramirez-Ruiz, E.; Cline, T.L.; Hurley, K. A Possible Cepheid-like Luminosity Estimator for the Long Gamma-Ray Bursts. *Astrophys. J.* **2001**, *552*, 57–71.
114. Fenimore, E.E.; Ramirez-Ruiz, E. Redshifts For 220 BATSE Gamma-Ray Bursts Determined by Variability and the Cosmological Consequences. *arXiv* **2000**, arXiv:astro–ph/0004176.
115. Yonetoku, D.; Murakami, T.; Nakamura, T.; Yamazaki, R.; Inoue, A.K.; Ioka, K. Gamma-Ray Burst Formation Rate Inferred from the Spectral Peak Energy-Peak Luminosity Relation. *Astrophys. J.* **2004**, *609*, 935–951.
116. Ghisellini, G.; Haardt, F.; Campana, S.; Lazzati, D.; Covino, S. Redshift Determination in the X-ray Band of Gamma-Ray Bursts. *Astrophys. J.* **1999**, *517*, 168–173.
117. D'Isanto, A.; Polsterer, K.L. Photometric redshift estimation via deep learning—Generalized and pre-classification-less, image based, fully probabilistic redshifts. *Astron. Astrophys.* **2018**, *609*, A111. [CrossRef]
118. Dainotti, M.; Petrosian, V.; Bogdan, M.; Miasojedow, B.; Nagataki, S.; Hastie, T.; Nuyngen, Z.; Gilda, S.; Hernandez, X.; Krol, D. Gamma-ray Bursts as distance indicators through a machine learning approach. *arXiv* **2019**, arXiv:1907.05074.
119. Lee, J.; Shin, M.S. Estimation of Photometric Redshifts. I. Machine-learning Inference for Pan-STARRS1 Galaxies Using Neural Networks. *Astron. J.* **2021**, *162*, 297.
120. Momtaz, A.; Salimi, M.H.; Shakeri, S. Estimating the Photometric Redshifts of Galaxies and QSOs Using Regression Techniques in Machine Learning. *arXiv* **2022**, arXiv:2201.04391.
121. Gruber, D.; Greiner, J.; von Kienlin, A.; Rau, A.; Briggs, M.S.; Connaughton, V.; Goldstein, A.; van der Horst, A.J.; Nardini, M.; Bhat, P.N.; et al. Rest-frame properties of 32 gamma-ray bursts observed by the Fermi Gamma-ray Burst Monitor. *Astron. Astrophys.* **2011**, *531*, A20.
122. Atteia, J.L.; Heussaff, V.; Dezalay, J.P.; Klotz, A.; Turpin, D.; Tsvetkova, A.E.; Frederiks, D.D.; Zolnierowski, Y.; Daigne, F.; Mochkovitch, R. The Maximum Isotropic Energy of Gamma-ray Bursts. *Astrophys. J.* **2017**, *837*, 119.
123. Minaev, P.Y.; Pozanenko, A.S. The $E_{p,I}$-E_{iso} correlation: Type I gamma-ray bursts and the new classification method. *Mon. Not. RAS* **2020**, *492*, 1919–1936. Erratum in *Mon. Not. RAS* **2021**, *504*, 926–927.
124. Lloyd-Ronning, N.M.; Fryer, C.L.; Ramirez-Ruiz, E. Cosmological Aspects of Gamma-Ray Bursts: Luminosity Evolution and an Estimate of the Star Formation Rate at High Redshifts. *Astrophys. J.* **2002**, *574*, 554–565.
125. Kocevski, D.; Liang, E. Quantifying the Luminosity Evolution in Gamma-Ray Bursts. *Astrophys. J.* **2006**, *642*, 371–381.
126. Ukwatta, T.N.; Woźniak, P.R.; Gehrels, N. Machine-z: Rapid machine-learned redshift indicator for Swift gamma-ray bursts. *Mon. Not. RAS* **2016**, *458*, 3821–3829.
127. Amati, L.; O'Brien, P.T.; Götz, D.; Bozzo, E.; Santangelo, A.; Tanvir, N.; Frontera, F.; Mereghetti, S.; Osborne, J.P.; Blain, A.; et al. The THESEUS space mission: Science goals, requirements and mission concept. *Exp. Astron.* **2021**, *52*, 183–218.
128. Ghirlanda, G.; Salvaterra, R.; Toffano, M.; Ronchini, S.; Guidorzi, C.; Oganesyan, G.; Ascenzi, S.; Bernardini, M.G.; Camisasca, A.E.; Mereghetti, S.; et al. Gamma ray burst studies with THESEUS. *Exp. Astron.* **2021**, *52*, 277–308.